A comparison of two CFD packages and engineering formulae for fluid flow problems

Report 96-93

R. Agtersloot
C. Vuik
M. Zijlema

TU Delft

Faculteit der Technische Wiskunde en Informatica
Faculty of Technical Mathematics and Informatics

Technische Universiteit Delft
Delft University of Technology

A comparison of two CFD packages and engineering formulae for fluid flow problems

R. Agtersloot [*]   C. Vuik [†]   M. Zijlema [‡]

Abstract

In this paper we compare CFD packages and engineering results for fluid flow problems, which occur in the thermal analysis of heat exchangers. Fluid flow problems are described by the well-known Navier-Stokes equations coupled with a number of transport equations. For large Reynolds numbers the resulting flow is turbulent. It is impossible to calculate a solution of the Navier-Stokes equations for a turbulent flow in a complicated 3D configuration in a reasonable time. For this reason engineering turbulence models are used. Some analytical results are known to approximate the solution of a flow problem. For more complicated turbulent flows only empirical relations are available. The coefficients in these formulae are obtained from experimental results. We compare the CFD results with each other and with the analytical and empirical results for simple geometries. Thereafter we show that CFD packages are able to compute results for problems where the engineering formulae are no longer valid. The CFD packages are: FLUENT, a commercial package used in industry, and ISNaS, a package developed in an academic environment.

Keywords: fluid flow problems, turbulence, heat transfer, CFD packages.

AMS Subject Classification: 65N05, 76D05, 80A20

1 Introduction and problem formulation

In this paper two CFD packages and engineering formulae are used to solve fluid flow problems. We start with a description of the Navier-Stokes equations for an incompressible

---

[*]Delft Hydraulics, Rotterdamseweg 185, 2629 CD Delft, The Netherlands

[†]Faculty of Technical Mathematics and Informatics, Delft University of Technology, Mekelweg 4, NL 2628 CD Delft, The Netherlands

[‡]Faculty of Technical Mathematics and Informatics, Delft University of Technology, Mekelweg 4, NL 2628 CD Delft, The Netherlands

flow. The Reynolds number characterises the properties of the flow. For small Reynolds numbers the flow is laminar, whereas for large Reynolds numbers the flow is turbulent. To predict a turbulent flow we use the so-called $k - \varepsilon$ turbulence model [14]. Since we are interested in heat exchange, we also present the energy equation.

We consider two dimensional flow of an incompressible fluid. In Cartesian co-ordinates the instationary Navier-Stokes equations are given by:

$$\frac{\partial \rho u_i}{\partial t} - \left(\frac{\partial \tau_{i1}}{\partial x_1} + \frac{\partial \tau_{i2}}{\partial x_2} \right) + \left(\frac{\partial \rho u_i u_1}{\partial x_1} + \frac{\partial \rho u_i u_2}{\partial x_2} \right) + \frac{\partial p}{\partial x_i} = 0, i \in \{1,2\}, (x_1, x_2) \in \Omega \quad (1)$$

where

$$\tau_{ii} = \mu \left(\frac{4}{3} \frac{\partial u_i}{\partial x_i} - \frac{2}{3} \frac{\partial u_j}{\partial x_j} \right), \quad \tau_{ij} = \mu \left(\frac{\partial u_i}{\partial x_j} + \frac{\partial u_j}{\partial x_i} \right), i, j \in \{1,2\}, i \neq j \quad (2)$$

together with the incompressibility condition

$$\frac{\partial u_1}{\partial x_1} + \frac{\partial u_2}{\partial x_2} = 0, (x_1, x_2) \in \Omega. \quad (3)$$

In these equations u_i is the component of the velocity of the fluid in x_i-direction, p is the pressure, τ_{ij} is the deviatoric stress tensor, ρ is the density, μ the dynamic viscosity, and Ω is the physical domain of interest.

We compute the flow in channel geometries. This implies that we have four different types of boundaries. Firstly fixed walls, with no slip conditions, i.e. both velocity components equal to zero. Secondly we have an inflow boundary. At this boundary the tangential velocity component u_t is equal to zero, whereas the normal velocity component u_n is given. Thirdly we have an outflow boundary. At this boundary often no physical information is available on which boundary conditions can be based. In order to avoid spurious wiggles we choose $\sigma_{nt} = \sigma_{nn} = 0$, where the total stress tensor is defined by $\sigma_{ij} = -p\delta_{ij} + \tau_{ij}$, $i, j \in \{n, t\}$ on the boundary. Finally we have a plane of symmetry, where we take: $u_n = \sigma_{nt} = 0$.

Only steady-state problems are considered. This implies that the choice of the initial condition is not important for the resulting stationary flow. However, the convergence of the transient solution depends on the initial condition. We always choose $u_i(x_1, x_2, 0) = 0, i \in \{1,2\}$ and $p(x_1, x_2, 0) = 0$.

The Reynolds number is given by

$$Re_D = \frac{\rho \bar{u} D}{\mu},$$

with $\bar{u}$ and D characteristic scales of the flow. For channels or ducts, D is the hydraulic diameter defined as $D = \frac{4A}{P}$, where A is the cross-sectional flow area and P is the wetted

perimeter. Furthermore, $\bar{u}$ is the average velocity at the inflow boundary. Beyond a Reynolds number of about 2000, channel flow becomes turbulent.

In turbulent flows the velocities remain fluctuating also in the stationary limit. It is very computer time and memory consuming to solve the Navier-Stokes equations such that these fluctuating velocities are approximated accurate enough. For this reason the velocity is split into a fluctuating part and a time averaged part. Time averaging the Navier-Stokes equations leads to equations for time averaged velocities. However, these equations contain the so-called turbulent Reynolds stresses, which depend on the fluctuating velocity field. This implies that the averaged equations are only easily solvable when the Reynolds stresses are given as a function of the time averaged velocities. One method to do this is the $k - \varepsilon$ turbulence model. In this model k is the turbulent kinetic energy per unit mass and ε is the dissipation rate of turbulent kinetic energy per unit mass. Both quantities satisfy a convection-diffusion equation with source terms and appropriate initial and boundary conditions. For more details we refer to [14] and [34], where further references can be found.

With respect to the boundary conditions for the time averaged Navier-Stokes equations we note that no differences occur at the inflow and outflow boundaries and planes of symmetry. At fixed walls, in principle, the no slip conditions may be selected. However, for a high Reynolds number the wall shear stress is computed using the so-called "law of the wall" to obviate integration through the near-wall layer, which is dominated by small scales due to viscous effects. This method is proposed in [14], whereas the theoretical background can be found in [12].

Since we are interested in heat exchange applications also the energy equation is specified. The temperature T satisfies:

$$\frac{\partial \rho c_p T}{\partial t} - \left(\frac{\partial}{\partial x_1} k_T \frac{\partial T}{\partial x_1} + \frac{\partial}{\partial x_2} k_T \frac{\partial T}{\partial x_2} \right) + \left(\frac{\partial \rho c_p u_1 T}{\partial x_1} + \frac{\partial \rho c_p u_2 T}{\partial x_2} \right) = 0, (x_1, x_2) \in \Omega, \quad (4)$$

where c_p is the specific heat at constant pressure and k_T is the thermal conductivity. The coefficients ρ, c_p, and k_T depend on the temperature. In our applications we take these coefficients as constants, because the temperature variations are small. As boundary conditions we give the temperature at the inflow boundary and the fixed walls. At the outflow boundary and a plane of symmetry we take the homogeneous Neumann condition for T, i.e. $\partial T / \partial \boldsymbol{n} = 0$, with $\boldsymbol{n}$ the unit outward pointing normal. For a turbulent flow we again use the "law of the wall" boundary conditions at the fixed walls [14].

The remainder of this paper is organised as follows. In Section 2 some analytical and engineering formulae are given to predict the pressure drop, velocities and temperature for relative simple geometries. A short description of the CFD packages is given in Section 3. Section 4 contains a comparison of the CFD results and engineering predictions. The conclusions of this comparison are summarised in Section 5.

3

2 Analytical and engineering formulae to predict some flow variables

In this section we summarise some formulae used in the engineering community to predict the pressure loss, velocity, and temperature distribution in incompressible duct flows.

2.1 Pressure drop for a flow in a pipe or duct

The pressure drop of a viscous incompressible flow in a pipe with length L and an hydraulic diameter D is given by ([22] p. 388):

$$\Delta p = f \frac{\rho \bar{u}^2 L}{2D}, \tag{5}$$

where $\bar{u}$ is the average velocity, where the averaging takes place at a cross-section of the channel. The friction factor f describes the influence of the pipe on the pressure drop due to the curvature, wall-roughness, velocity, etc. This formula is also valid for a flow between two flat plates. The distance between both plates is denoted by d_w. In this case the hydraulic diameter is equal to 2 times the distance between the plates ($D = 2d_w$).

For a laminar flow ($Re_D < 2 \cdot 10^3$) in a channel formed by two parallel plates the friction factor can be determined analytically ([22] p. 394):

$$f = \frac{96}{Re_D}. \tag{6}$$

The empirical friction factor for concentric annuli and rectangular ducts can be found in ([22] p. 392). For a rectangular duct we use:

$$f = \frac{64}{Re_D}. \tag{7}$$

For a turbulent flow the friction factor has to be determined experimentally. For a turbulent flow in a smooth circular pipe the following expression is used ([22] p. 457):

$$f = 0.184 Re_D^{-0.2}, \text{ where } 10^4 \leq Re_D \leq 10^5. \tag{8}$$

This formula is also valid for a flow between two flat plates.

Finally, to compute the pressure drop in a bent channel the influence of the bends should be taken into account. One method to do this is to use the concept of an equivalent length (L_{eq}) defined by

$$L_{eq} = \frac{k_L D}{f}, \tag{9}$$

4

where k_L is a loss coefficient, for which values can be found in the literature (see for instance [22] p. 462). In order to estimate the pressure drop for a bent channel one has to do the following: determine for each bend the loss coefficient, calculate the equivalent lengths and add them to L to obtain the total length (L_{tot}). Use L_{tot} in formula (5) to approximate the total pressure drop.

2.2   Velocity distribution for a flow between two plates

We consider a fluid flow entering a channel, which consists of two horizontal parallel plates. The velocity at the entrance is constant and equal to the averaged velocity $\bar{u}$. We assume that the flow is stationary. The no slip boundary conditions at the plates imply that the horizontal velocity drops to zero in the vicinity of the plates. The averaged velocity remains the same in every cross-section, since the flow is considered incompressible. For this reason the horizontal velocity at the centreline (the maximal velocity u_{max}) becomes larger than the averaged velocity.

After a certain length L_e, depending on various parameters, the velocity profile remains constant in the flow direction, so the flow region consists of two parts: the entrance region $(x \leq L_e)$ and the fully developed region $(x > L_e)$.

For a laminar flow it is well-known that the velocity profile is parabolic for $x > L_e$. It is easy to see that the horizontal velocity in the fully developed region is given by

$$u(y) = \frac{6y(d_w - y)}{d_w^2}\bar{u}, \quad y \in [0, d_w]. \tag{10}$$

This implies that $u_{max} = u|_{y=\frac{1}{2}d_w} = \frac{3}{2}\bar{u}$.

In the entrance region some approximate solutions are known. We use the results given in Section 9-18 of [7]. The velocity on the centreline is denoted by u_F. The following relation is derived (see [7], formula 9-181):

$$\frac{16x}{DRe_D} = 0.3 \left[9\left(\frac{u_F}{\bar{u}} - 1\right) - 16\ln\left(\frac{u_F}{\bar{u}}\right) - 7\left(\frac{\bar{u}}{u_F} - 1\right)\right]. \tag{11}$$

Substituting $u_{max} = \frac{3}{2}\bar{u}$ in (11) one obtains an expression for L_e:

$$L_e = 0.0065 \cdot Re_D \cdot D. \tag{12}$$

For turbulent flows no analytical results are available. However the following empirical formula can be used in the fully developed region [5]:

$$u_{max} = u|_{y=\frac{1}{2}d_w} = 1.25\bar{u}\left(\frac{\bar{u}d_w\rho}{\mu}\right)^{-0.0116}, \tag{13}$$

which is valid for $10^4 < Re_D < 10^6$.

5

2.3 Temperature distribution

In this section we consider a simple model to describe the temperature of a fluid flowing through a channel. The mass flow is denoted by ϕ_m $(= \rho \bar{u} A)$ and the wetted perimeter of the channel is P. We assume that the fluid temperature is constant in a cross section of the channel. Finally the wall temperature T_w is a given constant. The following differential equation can be used to describe the temperature:

$$\frac{dT}{dx} = \frac{-hP}{\phi_m c_p}(T - T_w), \tag{14}$$

where h is the average heat transfer coefficient. If the initial temperature is given by T_{in} then the integration of (14) yields:

$$T(x) = T_w + (T_{in} - T_w)\exp(\frac{-hP}{\phi_m c_p}x). \tag{15}$$

A problem that remains is: how to find an accurate approximation for the value of the average heat transfer coefficient h. It appears that h depends on the Reynolds number (Re_D) and the Prandtl number. The Prandtl number is the ratio between the momentum diffusivity and the thermal diffusivity and is given by $Pr_T = \frac{c_p \mu}{k_T}$. For a laminar flow the average heat transfer coefficient is approximated by the following empirical formula:

$$\frac{hD}{k_T} = 1.86 \left(Re_D \cdot Pr_T \cdot \frac{D}{L} \right)^{1/3}, \tag{16}$$

which is valid if $Re_D \cdot Pr_T \cdot \frac{D}{L} > 10$. We obtain (16) from [1] (equation (13.2-17)) using the assumption that the dynamic viscosity μ is a constant. The relative error in h appears to be less than 0.2 (see [1] p. 401).

For a turbulent flow with a high Reynolds number the Dittus-Boelter equation can be used ([22] p. 491):

$$\frac{hD}{k_T} = 0.023(Pr_T)^n(Re_D)^{0.8}, \tag{17}$$

where $n = 0.4$ for heating the fluid and $n = 0.3$ for cooling the fluid. The Dittus-Boelter relation is only valid if $10^4 < Re_D < 10^5$, $0.7 < Pr_T < 120$, and $L/D > 60$, where L is the length of the channel. The restriction on the ratio of L and D is a result of the development of the velocity and temperature profiles in the channel. If the inequality holds then the average heat transfer coefficient is more or less independent of L. If this inequality does not hold one has to modify the value of h in the entrance region (for details see [22]). Combination of (15) with (16) or (17) leads to an explicit (empirical) formula for the temperature of the fluid.

To compute the amount of heat exchange, we use the following formula:

$$\Delta Q = \rho c_p \left(\int_{\Gamma_{in}} u_n T \, d\Gamma - \int_{\Gamma_{out}} u_n T \, d\Gamma \right), \tag{18}$$

6

where u_n is the normal velocity and $\Gamma_{in}, \Gamma_{out}$ are respectively the inflow and outflow boundary. In a turbulent flow, it appears that a good approximation of ΔQ is obtained when the integrals are approximated by

$$\int_{\Gamma} u_n T \, d\Gamma \simeq \bar{u} \bar{T} A, \tag{19}$$

where $\bar{u}$ and $\bar{T}$ are the quantities averaged along Γ and A is the surface of Γ. If $A_{in} = A_{out}$ then the averaged velocity remains the same because the flow is incompressible. This combined with (18) and (19) leads to

$$\Delta Q \simeq \rho c_p \bar{u} A \left(\bar{T}_{in} - \bar{T}_{out} \right) = c_p \phi_m \left(\bar{T}_{in} - \bar{T}_{out} \right). \tag{20}$$

Substituting (15) for T_{out} in (20) one obtains

$$\Delta Q \simeq \rho c_p \bar{u} A \left(\bar{T}_{in} - \bar{T}_w \right) \left(1 - \exp \left(\frac{-hPL}{c_p \rho \bar{u} A} \right) \right).$$

It follows from (17) that h is proportional to $\bar{u}^{0.8}$. This combined with a first order Taylor expansion of exp shows that $\Delta Q \simeq c \bar{u}^{0.8}$.

3 A description of the CFD packages

In this section the main characteristics of the CFD packages used in this paper are outlined. These are the commercial code FLUENT and the academic code ISNaS.

3.1 A concise description of FLUENT

FLUENT is a general purpose Navier-Stokes solution package solving integral conservation equations for conservation of mass, momentum, energy and chemical species. The physical models in FLUENT can handle laminar and turbulent (in)compressible flows in stationary and time-dependent situations. These flow calculations can be combined with other transport equations. Some possible applications are conjugate heat transfer, chemically reacting flows, phase change in flows, free surface problems, sliding or deforming mesh problems and radiation problems.

The governing equations are discretized using a control-volume based method in which the governing equations are integrated over the control volumes. This integration is performed under several assumptions. All integrals are approximated by mean values, the convective terms are approximated by the first order power-law or second order QUICK schemes and the diffusive terms are approximated by central differences. FLUENT uses a non-staggered grid system in which Cartesian velocity components and scalars are stored at the centre of the control volumes. To avoid wiggles in the pressure solutions the "pressure weighted"

interpolation method of Rhie and Chow [19] is used. FLUENT uses the SIMPLE algorithm [18] to sequentially update all unknowns. This algorithm has the following form:

1 solve the momentum equations, based on the current guess for the pressure, and update velocities u_i,

2 solve the mass balance equation, in pressure-correction form, thereafter the pressure and velocities are updated,

3 solve all scalar equations (enthalpy, species, k, ε),

4 solve auxiliary equations (e.g. Reynolds Stress Model, radiation),

5 update fluid properties,

6 if un-converged goto 1.

The linear equations are solved by means of a line Gauss-Seidel iterative method or multi-grid solver. Reynolds stresses are modelled using the standard $k - \varepsilon$ model [14], a Re-Normalisation Group based $k - \varepsilon$ model [32] or the differential Reynolds Stress Model [13].

In transient calculations, the time-dependent conservation equations must be discretized in both space and time. The spatial discretization for the time-dependent equations is identical to the stationary case. Temporal discretization involves the integration of every term in the differential equations over a time step Δt. This integration is done by means of a fully implicit Euler scheme.

3.2   A concise description of ISNaS

The current capabilities of the ISNaS code include the simulations of laminar and turbulent flows, incompressible and compressible flows, steady-state and time-dependent flows, isothermal flows and flows with heat transfer in two- or three-dimensional complicated geometries. Furthermore, ISNaS may also be used to solve a number of "stand-alone" convection-diffusion equations, i.e. without solving the Navier-Stokes equations. Parallelization of the code on a cluster of HP workstations is based on domain decomposition and has been implemented with the public domain PVM (Parallel Virtual Machine) package [8].

The code is based on a co-ordinate invariant finite volume discretization on a staggered non-orthogonal multi-block grid of the incompressible Reynolds-averaged Navier-Stokes equations. These equations have to be recasted in a form in which both independent and dependent variables are invariant with respect to a change of co-ordinates. As a consequence, the formulation contains Christoffel symbols, which involve second derivatives of the co-ordinate mapping. For better accuracy, mass fluxes are used as primary unknowns

instead of the contra-variant velocity components. A list of relevant publications is [15], [29], [21], [16], [17], [28], [3], [33], [30], [36] and [35].

Turbulence modelling capabilities are primarily based on two-equation models. The two-equation models, both high- and low-Reynolds-number variants, in the current version of ISNaS include: the standard k-ε model of Launder and Spalding [14], the RNG based k-ε variant of Yakhot *et al.* [32], the extended k-ε model of Chen and Kim [4] and Wilcox's k-ω closure [31]. These models are used in conjunction with the linear (isotropic) Boussinesq eddy-viscosity model. In the near future, some well-known nonlinear (anisotropic) eddy-viscosity models will be implemented, for example the one proposed by Speziale [23]. The k-ω model is a low-Reynolds-number closure which means that it can be integrated through the viscous sub-layer without requiring a near-wall model. The three k-ε variants are of the high-Reynolds-number type and the viscosity-affected near wall region is resolved with a low-Reynolds-number model according to Lam and Bremhorst [11]. In this paper, however, for reasons of simplicity and economy, wall functions [14] are used instead of low-Reynolds-number modelling. Wall functions employ empirical laws to circumvent the inability of the k-ε type models to predict a logarithmic velocity profile near a wall. Hence, this approach can be used to provide near-wall boundary conditions for the momentum and turbulence transport equations, rather then on the wall itself, so that the viscous sub-layer does not have to be resolved. For stagnation flows, the so-called Kato-Launder modification [9], which replaces the strain in the production of turbulent energy term by the vorticity, has been implemented.

The governing equations are discretized with a finite volume method on a staggered grid in two (cf. Figure 1) or three dimensions. The momentum equations are integrated over a
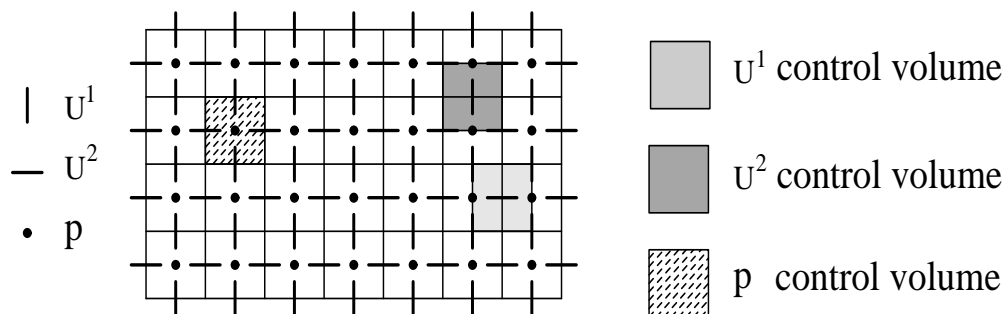

Figure 1: A staggered grid

U^α-cell to yield the equations containing unknown cell-face fluxes, which necessitates the use of central differences and bilinear interpolations. At this moment, the grid is assumed to be smooth. This assumption allows us to discretize the Christoffel symbols in a straightforward way. An extension to the non-smooth case is explained in [24]. Discretization of the turbulence transport equations is done similarly, except that the convection terms are

approximated with higher order flux-limiting schemes in order to avoid un-physical oscillations, typically in the vicinity of steep gradients. Otherwise, these "wiggles" tend to grow in an unbounded manner, which prevent the solutions to converge. Details on the flux-limiting technique may be found in [37].

Time discretization is done by the implicit Euler method and linearization is carried out with the Picard or Newton method. A second order pressure correction scheme [25] is used to obtain a divergence-free velocity field. The higher order flux-limiting schemes can easily be implemented by means of a defect correction approach [10]. The three linear systems, namely momentum, pressure and transport equations, are solved in each time step by a preconditioned GMRES solver [20]. For preconditioners we use incomplete LU factorizations. Further details may be found in [26, 27]. In every time step first the momentum and continuity equations are solved, followed by a number of transport equations (e.g. temperature) and then each turbulence equation. For a stationary problem, the time stepping is repeated until a stationary solution is achieved.

4 A comparison of the various solution methods

This section compares the results of the CFD simulations with the engineering predictions based on Section 2. The examples which are considered in this section are motivated by heat exchanger problems. The relatively simple geometries are: flow between two flat plates (2D), a U-shaped channel (2D), and a 3D square duct. Demirdzic *et al.* presented in [6] other bench mark problems for fluid flow and heat transfer.

Although various cases are considered (laminar and turbulent flow, straight and bent geometries, and 2D and 3D situations), throughout this section the fluid properties have the following values:

$$\rho = 10^3 \frac{kg}{m^3}, \qquad c_p = 4 \cdot 10^3 \frac{J}{kg\,^\circ C}, \qquad \mu = 10^{-3} \frac{kg}{m\,s}, \qquad k_T = 1 \frac{J}{m\,^\circ C\,s} \ .$$

This means that the Prandtl number for all the simulations will be $Pr_T = 4$. With respect to the turbulent flow calculations the standard k-ε model with wall functions has been used. The streamwise velocity u_{in} and the temperature at inflow are taken uniform, whereas k and ε are obtained from the formulae

$$k_{in} = 1.5 I_{\mathrm{T}}^2 u_{in}^2, \qquad \varepsilon_{in} = \frac{c_\mu^{3/4} k_{in}^{3/2}}{l} \ . \tag{21}$$

Here, I_{T} is the turbulence intensity, taken to be 1%, $c_\mu (= 0.09)$ is an empirical constant used in the k-ε model, and l is the mixing length given by:

$$l(y) = \min(\kappa \cdot y, 0.1D) \ , \tag{22}$$

where $\kappa(= 0.4)$ is the Von Karmann constant used in the "law of the wall". In addition, wall functions, symmetry and out-stream conditions are imposed in the usual way. The fluid inlet temperature T_{in} is $50^o C$, and the wall temperature T_w is $30^o C$. The fluid outlet temperature is the "cup-mixing" temperature, i.e. we collect the fluid at the outlet, mix it thoroughly and measure its temperature.

When we compare different temperature results it is a priori not clear how these differences should be scaled. There are various reference temperatures which can be used: $T_w, T_{in}, T_{in} - T_w$, etc. Since in our problems (heat exchangers) it is important to know how much heat is exchanged we define the "relative difference" between two approximations $\bar{T}$ and $\hat{T}$ as

$$\frac{|\bar{T} - \hat{T}|}{T_{in} - \max\{\bar{T}, \hat{T}\}} \quad . \tag{23}$$

Some of the figures in this section (see for example Figure 2) have a label "x-distance" or "y-distance". The quantity x-distance is the distance from the inlet of the channel measured in the direction of the flow, whereas the y-distance is the distance from the lower plate perpendicular to this plate. Figures which show results obtained with ISNaS are drawn with a '−' line and results obtained with FLUENT are drawn with a '-.' line.

4.1 Heat transfer for a laminar flow between two flat plates

This section contains the results of laminar flow simulations in a channel consisting of two parallel plates. This channel is 10m long and 0.05m wide. The equidistant grid consists of 20 cells in the y-direction, and 200 cells in the x-direction. Simulations are carried out with five different fluid velocities, ranging from 0.001 till 0.02 ms^{-1}. Thus the resulting Reynolds numbers, based on the hydraulic diameter $(0.1m)$ range from 10^2 till $2 \cdot 10^3$.

The amount of heat transferred from the fluid to the wall is denoted by ΔQ. This quantity is computed by formula (18), in which the integral of the product of $u_n \cdot T$ is computed with the trapezium rule.

According to formulae (16) the engineering prediction of the heat transfer coefficient h is given by $h = 295 \cdot (\bar{u})^{\frac{1}{3}}$. Substituting this value into (15) gives the engineering outflow temperature

$$T_{out} = 30 + 20 \exp(-0.0295\overline{u}^{-\frac{2}{3}}).$$

Table 1 shows the results for the five velocities indicated. The agreement between the ISNaS and FLUENT results in Table 1 is found again in Figure 2, which shows the temperature along the centreline for the five different situations. Figures 3 and 4 show the temperature profiles at 1m, 5m and 10m from the inlet, and the temperature profiles along the centreline in the channel for $Re_D = 2 \cdot 10^3$. Note the profile development from a

11

$\overline{u}\,(ms^{-1})$	Re_D	$T_{out}\,(^{o}C)$			$\Delta Q\,(\times 10^3\,W)$		
		engineering	ISNaS	FLUENT	engineering	ISNaS	FLUENT
$1 \cdot 10^{-3}$	$1 \cdot 10^{2}$	31.05	30.00	30.01	3.8	4.0	4.0
$2 \cdot 10^{-3}$	$2 \cdot 10^{2}$	33.12	30.18	30.42	6.8	7.9	7.8
$5 \cdot 10^{-3}$	$5 \cdot 10^{2}$	37.29	33.83	33.94	12.7	16.2	16.1
$1 \cdot 10^{-2}$	$1 \cdot 10^{3}$	40.59	38.24	38.39	18.8	23.5	23.2
$2 \cdot 10^{-2}$	$2 \cdot 10^{3}$	43.40	42.21	42.28	26.4	31.2	30.9

Table 1: Engineering, ISNaS and FLUENT results for a laminar channel flow

partially uniform pattern (Figure 3a) to a fully laminar parabolic pattern (Figure 4a). Although the difference in the fluid temperature along the centreline (Figure 4b) seems to be considerable, the relative difference is only $3.5 \cdot 10^{-3}$. The velocity fields show even more resemblance than the temperature fields. This can be seen in Figures 5 and 6. Note again the development from a uniform flow profile (Figure 5a) to a fully laminar flow profile (Figure 6a).
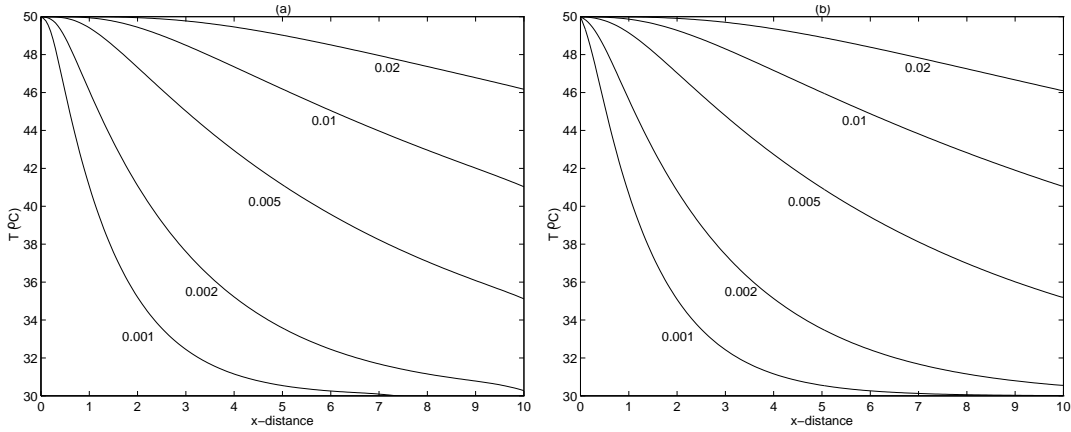

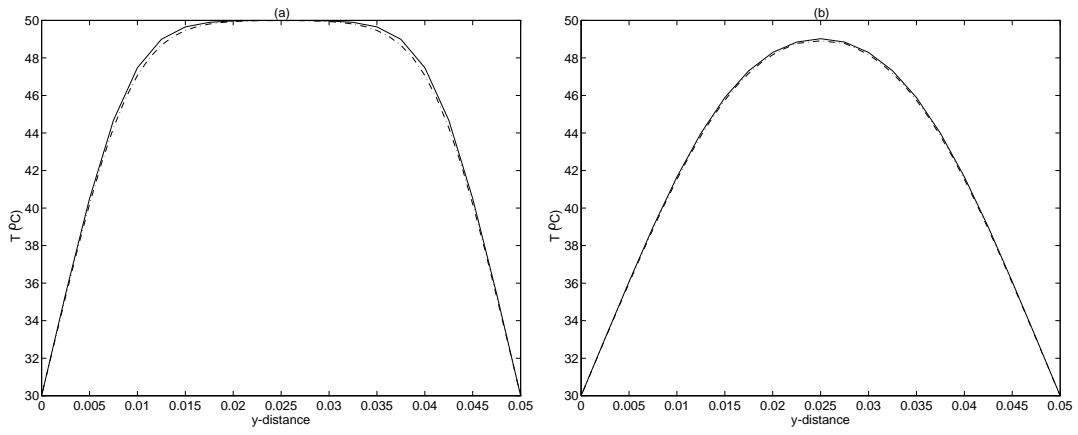Figure 2: The temperature profiles for various choices of u_{in}: (a) by ISNaS; (b) by FLUENT

Figure 3: Temperature profiles: (a) at $1.0m$ from the inlet; (b) at $5.0m$ from the inlet
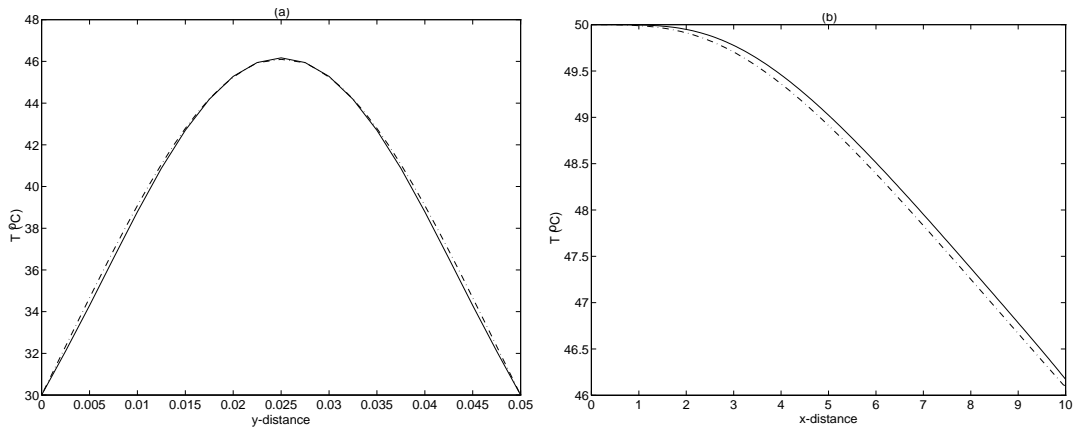

Figure 4: Temperature profiles: (a) at the outlet; (b) along the centreline
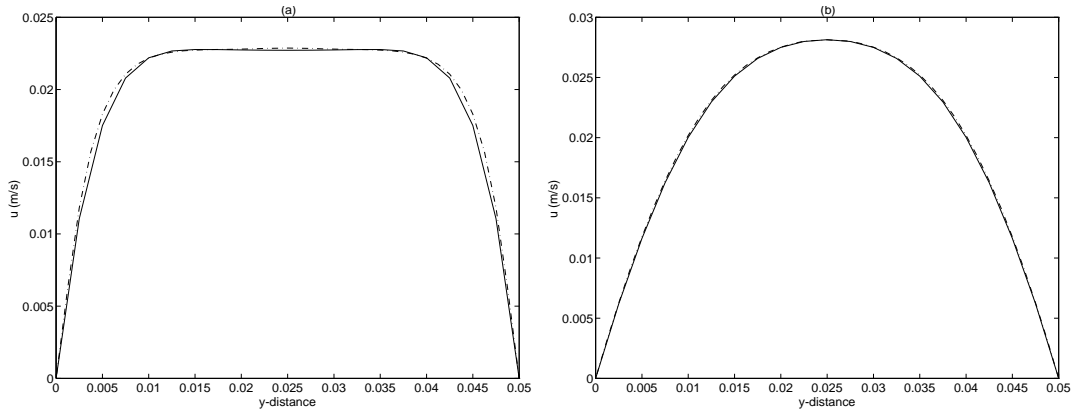
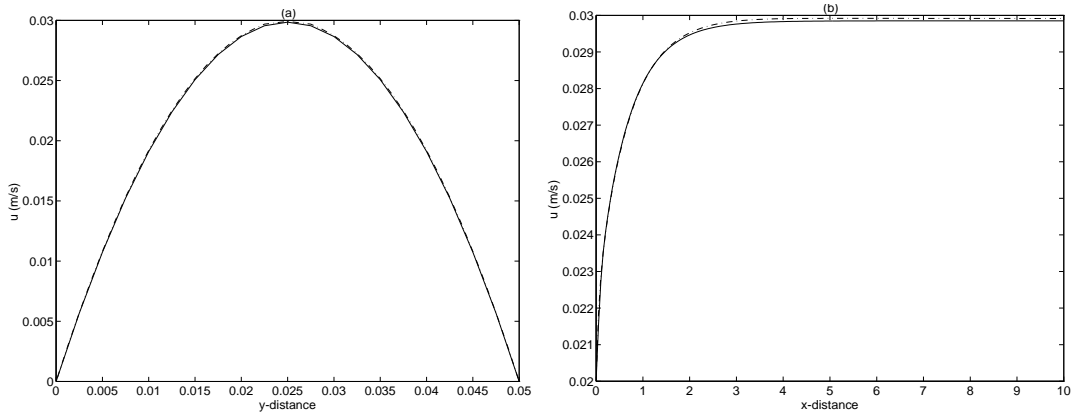Figure 5: Velocity profiles: (a) at $0.1m$ from the inlet; (b)at $1.0m$ from the inlet

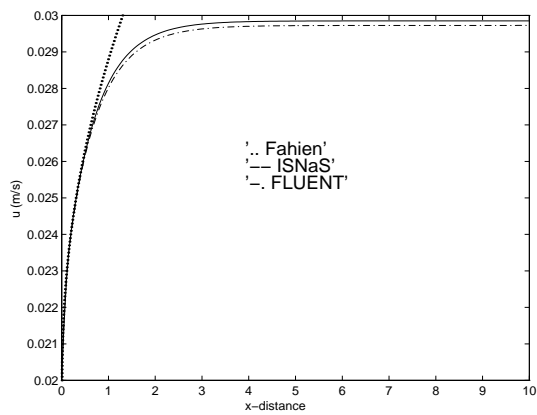Figure 6: Velocity profiles: (a) at the outlet; (b) along the centreline

Figure 7: Development from uniform to fully laminar flow

We can draw several conclusions from these simulations.

- The relative difference between the engineering prediction of T_{out} and those obtained from ISNaS and FLUENT is approximately 0.25. This is correct within the bounds given in ([1] p. 401), where is stated that formula (16) can underestimate the actual heat transfer coefficient with 20%.

- The relative difference between the temperature fields computed by ISNaS and FLUENT is less than 0.015 in all five simulations. The relative difference between the velocity fields from ISNaS and FLUENT is less than 0.005 in these simulations.

- In Section 2.2 it has been shown that $u_{max} = \frac{3}{2}\bar{u}$. This relationship holds also for ISNaS and FLUENT (see Figure 6b). The relative error between the analytical u_{max} and the computed u_{max} is less than 0.005.

- The final conclusion regards the development from a uniform flow pattern to a fully laminar flow pattern. Figure 7 shows the velocity at the centreline in the channel. The dotted line is the velocity development according to formula (11), the solid line is the velocity development computed by ISNaS, and the dashed line is the velocity development computed by FLUENT. Note that in the entrance region ($x \leq 0.5m$) the three profiles are the same.

4.2   Heat transfer for a turbulent flow between two flat plates

This section describes a turbulent flow in a channel. The geometry and the grid are similar to the geometry and the grid used in Section 4.1. Simulations are carried out with an inlet velocity ranging from 0.1 till 5 ms^{-1}, resulting in a Reynolds number ranging from 10^4 up to $5 \cdot 10^5$.

4.2.1   The results for the pressure drop and velocity

The engineering pressure drop (5) will be compared with the pressure drop computed by ISNaS and FLUENT for six different situations. The engineering pressure drop (based on (5), (8) and the hydraulic diameter of 0.1 m) is

$$\Delta p = 920 \cdot \bar{u}^{1.8}, \tag{24}$$

which is valid for $10^4 \leq Re_D \leq 10^5$. These simulations will also be used to verify equation (13) from Section 2.2.

15

u_{in}	Re_D	Δp			u_{max}		
		engineering	ISNaS	FLUENT	equation (13)	ISNaS	FLUENT
0.1	$1 \cdot 10^4$	15	20	30	0.1144	0.1136	0.1183
0.2	$2 \cdot 10^4$	51	53	72	0.2263	0.2245	0.2297
0.5	$5 \cdot 10^4$	264	268	274	0.5574	0.5547	0.5610
1.0	$1 \cdot 10^5$	920	924	925	1.1026	1.1012	1.1151
2.0	$2 \cdot 10^5$	3200	3270	3150	2.1808	2.1883	2.2167
5.0	$5 \cdot 10^5$	16670	16900	16680	5.3727	5.4311	5.5154

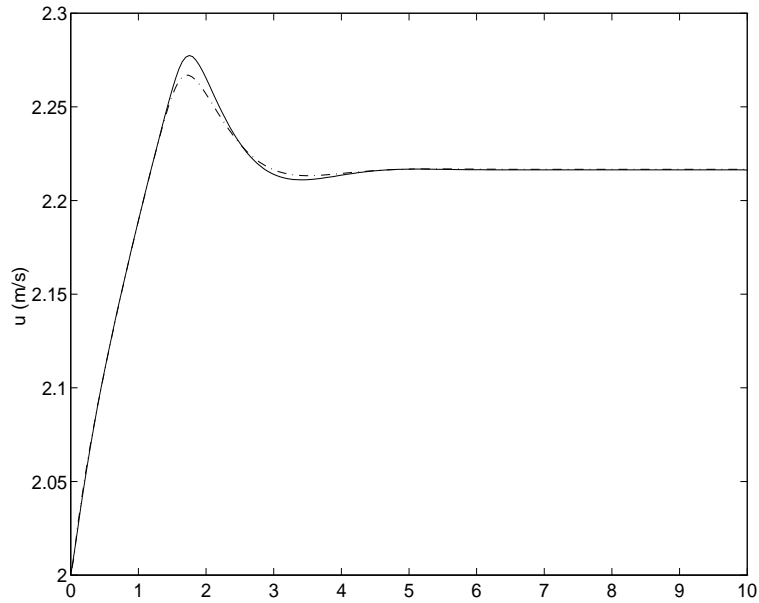Table 2: Engineering, ISNaS and FLUENT results for the turbulent channel flow

Figure 8: Velocity profiles along the centreline

Similar as in the previous section the velocity fields from both CFD packages are almost equal. A good example of this agreement is given in Figure 8. The "hills" in the velocity profile have almost the same height (relative difference is $4.8 \cdot 10^{-3}$) and have the same location. The results from ISNaS and FLUENT differ the most when the Reynolds number is relatively low. This is probably due to the use of the high Reynolds number $k - \varepsilon$ model, which gives the best results for very large Reynolds numbers. Equation (13) is in accordance with the CFD results, as can be seen in Table 2. The relative difference is less than 0.027 for the FLUENT results, and less than 0.011 for the ISNaS results.

4.2.2 Heat transfer results

We have also considered turbulent flow in the channel combined with heat transfer. Both packages use the "law of the wall" for the transport of heat from the fluid to the walls. The T_{out} as given by ISNaS and FLUENT will be compared with an engineering prediction of T_{out}. According to formula (17) the heat transfer coefficient h is: $h = 3500 \cdot \overline{u}^{0.8}$. This results in an outflow temperature which depends on the velocity as follows:

$$T_{out} = 30 + 20 \exp(-0.35 \cdot \overline{u}^{-0.2}).$$
(25)

The geometry and fluid velocities are the same as in Section 4.2.1. Results are presented in Table 3. The ISNaS and FLUENT results agree rather well with each other, but they underestimate the engineering T_{out} with a relative difference of 0.3. An exception is the case with $Re_D = 10^4$, where FLUENT overestimates the heat transfer with almost 70%.

u_{in}	Re_D	T_{out}			relative difference	
		engineering	ISNaS	FLUENT	ISNaS	FLUENT
0.1	$1 \cdot 10^4$	41.48	39.06	35.60	0.284	0.690
0.2	$2 \cdot 10^4$	42.34	40.17	40.10	0.283	0.292
0.5	$5 \cdot 10^4$	43.38	41.51	41.65	0.283	0.261
1	$1 \cdot 10^5$	44.09	42.59	42.47	0.254	0.274
2	$2 \cdot 10^5$	44.75	43.36	43.16	0.265	0.303
5	$5 \cdot 10^5$	45.52	44.03	43.93	0.333	0.355

Table 3: Engineering, ISNaS and FLUENT results for turbulent heat transfer in a channel, together with the relative difference between the CFD results and the engineering prediction

4.3 Turbulent flow through a U-shaped channel

This section is concerned with the application of the CFD packages to the prediction of flow through a two-dimensional U-shaped channel as shown in Figure 9. Such a flow occurs
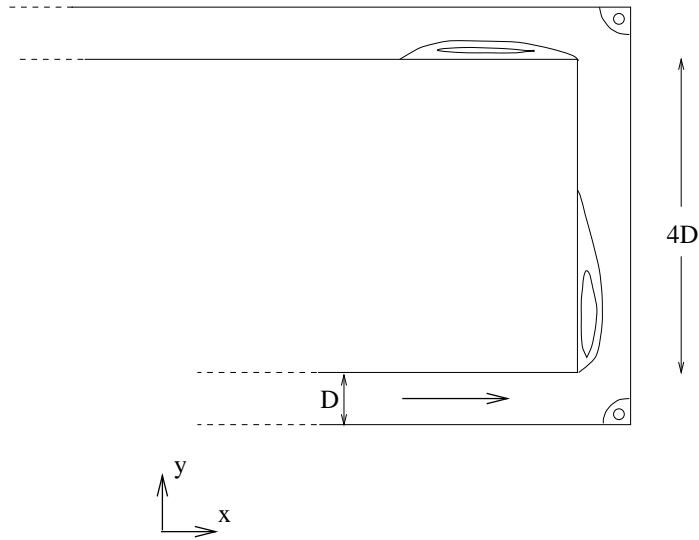
Figure 9: Flow geometry for the U-shaped channel with the indication of the recirculating zones

for example in cooling passages within gas-turbine blades. The geometry considered here has two 90° kinks, which cause separations. The width of the duct is $D = 0.05$ m. The Reynolds number based on the hydraulic diameter and the centreline inflow velocity u_{in} given below range from 10^4 up to $5 \cdot 10^5$. The inflow and outflow boundaries are located at 99 duct widths upstream and downstream of the 90° kinks, respectively.

In the computations, a multi-block approach combined with an orthogonal grid has been employed. Figure 10 shows the grid which consists of 3400 cells. For more details on the
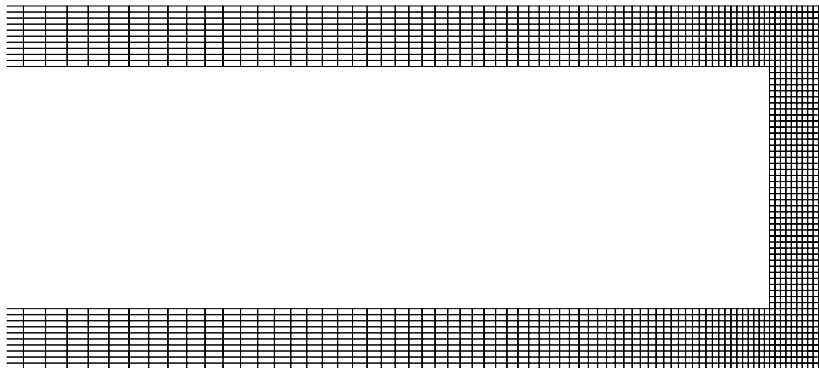

Figure 10: A part of the grid for the U-shaped channel

multi-block method as implemented in ISNaS, we refer to [2]. Systematic grid refinement tests have not been performed, instead it was assumed that the grid selected would be

suitable for this case.

Contour plots of streamlines corresponding to $u_{in} = 5\ ms^{-1}$ are shown in Figure 11. The streamlines show the expected behaviour and also indicate that the length of the largest
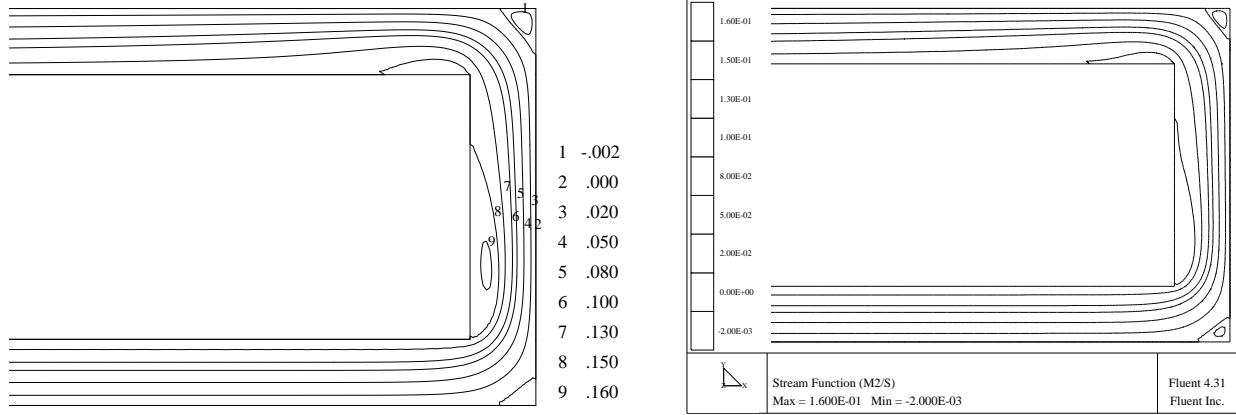

Figure 11: Streamlines for flow through U-shaped channel computed by ISNaS (left) and FLUENT (right)

recirculation zone is about three duct widths. However, one should keep in mind that the predicted recirculation regions may be too small, because the standard k-ε model is not capable of predicting effects of curvature on the turbulence. Also, one can see close resemblance between ISNaS and FLUENT results.

The calculated pressure drops and cup-mixing temperatures are compared with the engineering formulae given in Section 2. In Table 4 we present the pressure drop through the

u_{in}	Re_D	$\Delta p\,(Pa)$		
		engineering	ISNaS	FLUENT
0.1	$1 \cdot 10^4$	25	28	29
0.2	$2 \cdot 10^4$	91	103	89
0.5	$5 \cdot 10^4$	514	546	471
1.0	$1 \cdot 10^5$	1918	2140	1698
2.0	$2 \cdot 10^5$	7188	7335	6225
5.0	$5 \cdot 10^5$	41503	44761	34831

Table 4: Engineering and CFD predictions for pressure drops in turbulent flow through a U-shaped channel

U-shaped channel. The influence of the kinks on the pressure drop is described by the loss

19

coefficient k_L in (9). According to [22], for one 90° kink, $k_L = 0.98$. Hence, the equivalent length of two kinks is given by $L_{eq} = 10.65 \cdot \overline{u}^{0.2}$. Using (5), the engineering formula for the pressure drop is

$$\Delta p = 92 \cdot \overline{u}^{1.8}(L_b + L_{eq}) \ . \tag{26}$$

This formula is valid for $10^4 \leq Re_D \leq 10^5$. The quantity L_b is the length of the U-shaped channel and is determined by the average of the lengths of inner and outer walls. Thus, with $L_b = 10.2$ m, we have

$$\Delta p = 938.4 \cdot \overline{u}^{1.8} + 980 \cdot \overline{u}^2 \ . \tag{27}$$

The results show that both CFD packages can handle the U-shaped channel. Furthermore, the calculated pressure drop of ISNaS is larger than the engineering prediction, while that of FLUENT is smaller. The relative difference between the engineering prediction and the computed pressure drop is less than 0.16 for FLUENT, and less than 0.13 for ISNaS. The length of the U-shaped channel is approximately the same as the length of the channel considered in Section 4.2. Comparing the pressure in tables 2 and 4, it appears that the 90° kinks have a considerable influence on the pressure.

In Table 5 the computed temperatures are presented at the outlet of the U-shaped channel.

u_{in}	Re_D	T_{out} (^oC)			relative difference	
		engineering	ISNaS	FLUENT	ISNaS	FLUENT
0.1	$1 \cdot 10^4$	41.38	39.40	39.60	0.23	0.21
0.2	$2 \cdot 10^4$	42.25	39.78	40.19	0.32	0.27
0.5	$5 \cdot 10^4$	43.29	41.23	41.39	0.31	0.28
1.0	$1 \cdot 10^5$	44.02	42.05	42.15	0.33	0.31
2.0	$2 \cdot 10^5$	44.68	42.74	42.81	0.36	0.35
5.0	$5 \cdot 10^5$	45.46	43.14	43.58	0.51	0.41

Table 5: Engineering and CFD predictions for cup-mixing temperatures in turbulent flow through a U-shaped channel

Unfortunately, we have not found engineering formulae for flow with heat transfer through tube systems with appendages. Therefore, we calculate the engineering prediction for the cup-mixing temperature of a straight channel of length 10.2 m. The relative difference between engineering predictions and temperatures computed with the ISNaS and FLUENT packages are less than 0.51 and 0.41, respectively. We expect a considerable influence of the 90° kinks on the temperature. So, in our opinion the CFD results are closer to the physical values than the engineering predictions for the straight channel.

If we compare the outlet temperature computed by FLUENT from Table 5 with the outlet

temperature computed by FLUENT from Table 3 we see that the outlet temperature in the former case is approximately 5% lower for $Re_D \geq 10^5$, and 3% higher for $Re_D \leq 2 \cdot 10^4$. The same holds for ISNaS with 5% and 1%, respectively.

4.4   Laminar flow through a 3D square duct with heat transfer

One of the simplest examples of three-dimensional incompressible flow, either laminar or turbulent, in applications with heat transfer is a fully developed flow in a 3D square duct. The square duct is 0.05 m high, 0.05 m wide and 10 m long. Due to symmetry, only a quarter of the duct needs to be considered, i.e. 0.025 m high and 0.025 m wide. The computations were performed with a uniform grid consisting of $10 \times 10 \times 100$ cells. Based on the grid dependence test it was found that this grid is fine enough. The following experiments are done with a varying velocity at the inlet side, ranging from 0.001 up to 0.02 ms^{-1}. This means that the Reynolds numbers based on the hydraulic diameter of 0.05 m range from 50 till 1000.

We compare the computed pressure drops and cup-mixing temperatures with the engineering predictions given by the following formulae:

$$\Delta p = 128\,\overline{u}, \quad T_{out} = 30 + 20\exp(-0.0744\overline{u}^{-2/3})\,. \tag{28}$$

Inspection of Table 6 shows that ISNaS predicts a lower pressure drop (difference less

$u_{in}\,(ms^{-1})$	$\Delta p\,(Pa)$			$T_{out}\,(^oC)$		
	engineering	ISNaS	FLUENT	engineering	ISNaS	FLUENT
$1 \cdot 10^{-3}$	0.128	0.114	0.112	30.01	30.00	30.00
$2 \cdot 10^{-3}$	0.256	0.228	0.228	30.18	30.01	30.04
$5 \cdot 10^{-3}$	0.640	0.582	0.579	31.57	31.40	31.28
$1 \cdot 10^{-2}$	1.280	1.198	1.193	34.03	34.68	33.90
$2 \cdot 10^{-2}$	2.560	2.538	2.527	37.29	38.74	38.53

Table 6: Engineering and CFD predictions of pressure drops and cup-mixing temperatures for laminar square duct flow

than 11%) for the five Reynolds numbers indicated. Furthermore, the maximal relative difference between the computed cup-mixing temperatures and the engineering predictions is less than 0.13. The FLUENT results are comparable. Note that the relatively largest difference between engineering and CFD predictions for the pressure drop occurs at the lowest Reynolds number. The opposite is true for the cup-mixing temperature.

4.5 Turbulent flow through a 3D square duct with heat transfer

The geometry and the grid we used to test ISNaS and FLUENT for turbulent flows with heat transfer in a three-dimensional configuration is the same as in Section 4.4. The $100 \times 10 \times 10$ grid results were taken as acceptably grid independent and are presented below. Simulations are carried out with an inlet velocity ranging from 0.1 till 2 ms^{-1}, resulting in a Reynolds number, based on the hydraulic diameter (= 0.05 m), ranging from $5 \cdot 10^3$ up to 10^5.

The engineering prediction for the pressure drop according to formula (5) equals

$$\Delta p = 2114 \cdot \overline{u}^{1.8}, \tag{29}$$

which is valid for $10^4 \leq Re_D \leq 10^5$. The empirical heat transfer coefficient h depends on the velocity as follows: $h = 4005 \cdot \overline{u}^{0.8}$. Based on this result the engineering prediction for the cup-mixing temperature is given by

$$T_{out} = 30 + 20 \exp \left(-0.8\overline{u}^{-0.2} \right). \tag{30}$$

The computed pressure drops and cup-mixing temperatures are presented together with the engineering predictions in Table 7. Concerning the cup-mixing temperatures, both CFD

$u_{in} \left(ms^{-1} \right)$	$\Delta p \left(Pa \right)$			$T_{out} \left({}^{o}C \right)$		
	engineering	ISNaS	FLUENT	engineering	ISNaS	FLUENT
0.1	34	42	40	35.63	35.31	34.85
0.2	117	116	120	36.63	36.16	35.89
0.5	607	578	560	37.98	36.58	37.17
1.0	2112	1986	1920	38.99	37.62	38.07
2.0	7356	6885	6621	39.97	38.80	38.90

Table 7: Engineering and CFD predictions of pressure drop and cup-mixing temperature in turbulent square duct flow

predictions are in accordance with the engineering data. The maximal relative differences in case of ISNaS and FLUENT are 0.12 and 0.11, respectively. It can also be seen from the table that differences between computed and engineering predicted pressure drops nowhere exceed 10% for this case. Furthermore, the agreement between the ISNaS and FLUENT results can be said to be satisfactory. As no great surprise, the k-ε model is quite accurate for the duct flow.

It should be noted that ISNaS used the second order TVD/ISNAS scheme and FLUENT employed the first order power law scheme for solving the turbulence equations. Because

the CFD predictions are more or less the same, it seems that the solutions are insensitive to the accuracy of the approximation of the convective terms in the k-ε model. A possible explanation is the fact that the convective mechanism is of minor importance to the balance of turbulent processes, in which the production and dissipation rates are dominant [34].

4.6   Computational requirements for ISNaS and FLUENT

In order to compare the cost of computations of both ISNaS and FLUENT, these codes have been implemented on a Silicon Graphics computer (VGX, 100MHz, 96 Mbyte) at Delft Hydraulics. We discuss two test cases reported in this work to illustrate the comparison and its outcome: the turbulent flow through a U-shaped channel with $Re = 10^5$ and the laminar flow through a 3D square duct with $Re = 10^3$ on a $10 \times 10 \times 200$ grid.

Computational requirements are summarised in Table 8 giving, for each code separately,

test case	CPU time/time-step		required memory	
	ISNaS	FLUENT	ISNaS	FLUENT
2D (Sec. 4.3)	2.3	12	1.7	4.2
3D (Sec. 4.4)	145	100	18.8	7

Table 8: Averaged CPU times (seconds) per time step and memory (Mb).

the averaged CPU time for one time step and memory needed for building and solving the equations. The CPU time has been measured in seconds, whereas the memory size is given in megabytes. The main features deserved to be highlighted are the fact that, first, the CPU times corresponding to ISNaS are far lower than those of FLUENT for two dimensional problems, whereas FLUENT is more efficient for three dimensional problems; second, the amount of required memory is proportional to the number of cells times the size of the discretization stencil; and third, in three dimensions, ISNaS needs more memory than FLUENT, but in two dimensions, a reverse result has been observed. This can be explained as follows. In three dimensions, the total number of variables linked together in a momentum equation is 51 in ISNaS, whereas only 7 velocity points in the momentum equation are needed in FLUENT. In two dimensions, we have 13-point and 5-point stencils in ISNaS and FLUENT, respectively. Hence, in terms of the ratio of the size of the ISNAS to the FLUENT stencil, the demand on memory in ISNaS becomes quite considerable in a three dimensional problem.

When the solution is advanced, iteratively, towards the steady state, FLUENT required 3.9 s per iteration step using 4 Mb in the case of the 2D problem and for the 3D one, 19 s per iteration step with 7 Mb are needed. At this moment ISNaS does not contain any special methods to compute stationary solutions.

5   Conclusions

In this paper we compare two different CFD packages: FLUENT and ISNaS with results obtained from engineering predictions. From this comparison we draw the following conclusions.

The differences between the CFD results and the engineering predictions are reasonably small. An advantage of an engineering formula is that the results are cheap to compute. Furthermore it leads to insights in the dependence of the velocity, pressure drop and temperatures on various parameters. Disadvantages are: the range of applicability is restricted with respect to the Reynolds number and the geometry of the problem. Finally, it can be hard to obtain the correct formula from the large amount of literature.

The differences in the velocities and pressure drop are small, whereas the differences in the temperatures are somewhat larger. For the applications we have in mind (heat exchanger) these differences may be important. It would be nice to compare the numerical/engineering data with measurements to conclude which results are the best.

With respect to turbulent flows we note that there is a good correspondence between the numerical and engineering predictions. This implies that this type of problems is suitable for the $k - \varepsilon$ turbulence model.

In both CFD packages different numerical methods are used. However, the velocity, pressure, and temperature results are more or less the same. So it is not possible to discriminate the packages with respect to accuracy. An advantage of FLUENT is that it is somewhat easier to use and it has a wider range of applicability. An advantage of ISNaS is that the source code is available so it is possible to check the numerical methods used, or to adapt certain parts of the software. For instationary problems we see that in 2D the computational requirements for ISNaS are much less than for FLUENT. In 3D problems FLUENT is more efficient. In general the time step should be taken smaller in FLUENT than in ISNaS. Finally an advantage of FLUENT is that it has special techniques to solve stationary problems. In ISNaS stationary problems are solved via time stepping. Since no automatic time step strategy is used, much CPU time is needed if a wrong time step is chosen.

Acknowledgment

References

[1] R.B. Bird, W.E. Stewart, and E. N. Lightfoot. *Transport Phenomena*. John Wiley & Sons, New York, 1960.

[2] E. Brakkee. *Domain decomposition for the incompressible Navier-Stokes equations*. PhD thesis, Delft University of Technology, Delft, 1996.

[3] E. Brakkee, A. Segal, and C.G.M. Kassels. A parallel domain decomposition algorithm for the incompressible Navier-Stokes equations. *J. Simul. Pract. Theor.*, 3:185–205, 1995.

[4] Y.-S. Chen and S.-W. Kim. Computations of turbulent flows using an extended k-ε turbulence closure model. Contractor report NASA CR-179204, NASA-Marshall Space Flight Center, Alabama, USA, 1987.

[5] R.B. Dean. Reynolds number dependence of skin friction and other bulk flow variables in two-dimensional rectangular duct flow. *ASME J. of Fluids Engng, Ser. D*, 100:215, 1978.

[6] I. Demirdzic, Z. Lilek, and M. Peric. Fluid flow and heat transfer test problems for non-orthogonal grids: bench-mark solutions. *Int. J. Num. Meth. Fluids.*, 15:329–354, 1992.

[7] R.W. Fahien. *Fundamentals of Transport Phenomena*. McGraw-Hill Book Company, New York, 1983.

[8] A. Geist, A. Beguelin, J. Dongarra, W. Jiang, R. Manchek, and V. Sunderam. *PVM: Parallel Virtual Machine: a users' guide and tutorial for network parallel computing*. The MIT Press, Cambridge, 1994.

[9] M. Kato and B.E. Launder. The modelling of turbulent flow around stationary and vibrating square cylinders. In *Proc. Ninth Symposium on Turbulent Shear Flows*, page 10.4.1, Kyoto, Japan, 1993.

[10] P. K. Khosla and S. G. Rubin. A diagonally dominant second-order accurate implicit scheme. *Comput. Fluids*, 2:207–209, 1974.

[11] C.K.G. Lam and K. Bremhorst. A modified form of the k-ε model for predicting wall turbulence. *ASME J. Fluids Engng.*, 103:456–460, 1981.

[12] B.E. Launder. Turbulence modeling in the vicinity of a wall. In S.J. Kline, B.J. Cantwell, and G.M. Lilley, editors, *Complex turbulent flows: comparison of computation and experiment*, volume II, pages 691–699, Stanford University Press, Stanford, CA, 1982.

[13] B.E. Launder, G.J. Reece, and W. Rodi. Progress in the Development of a Reynolds-Stress Turbulence Closure. *J. Fluid. Mech*, 68:537–566, 1975.

[14] B.E. Launder and D.B. Spalding. The numerical computation of turbulent flows. *Comp. Methods Appl. Mech. Eng.*, 3:269–289, 1974.

[15] A.E. Mynett, P. Wesseling, A. Segal, and C.G.M. Kassels. The ISNaS incompressible Navier-Stokes solver: invariant discretization. *Applied Scientific Research*, 48:175–191, 1991.

[16] C.W. Oosterlee and P. Wesseling. A robust multigrid method for a discretization of the incompressible Navier-Stokes equations in general coordinates. *Impact Comp. Science Engng.*, 5:128–151, 1993.

[17] C.W. Oosterlee, P. Wesseling, A. Segal, and E. Brakkee. Benchmark solutions for the incompressible Navier-Stokes equations in general co-ordinates on staggered grids. *Int. J. Num. Meth. Fluids*, 17:301–321, 1993.

[18] S.V. Patankar and D.B. Spalding. A calculation procedure for heat and mass transfer in three-dimensional parabolic flows. *Int. J. Heat Mass Transfer*, 15:1787–1806, 1972.

[19] C.M. Rhie and W.L. Chow. Numerical study of the turbulent flow past an airfoil with trailing edge separation. *AIAA Journal*, 21:1525–1532, 1983.

[20] Y. Saad and M.H. Schultz. GMRES: a generalized minimal residual algorithm for solving non-symmetric linear systems. *SIAM J. Sci. Stat. Comp.*, 7:856–869, 1986.

[21] A. Segal, P. Wesseling, J. Van Kan, C.W. Oosterlee, and K. Kassels. Invariant discretization of the incompressible Navier-Stokes equations in boundary fitted co-ordinates. *Int. J. Num. Meth. Fluids*, 15:411–426, 1992.

[22] L.E. Sissom and D.R. Pitts. *Elements of transport phenomena*. McGraw-Hill, New York, 1972.

[23] C.G. Speziale. On nonlinear k-l and k-ε models of turbulence. *J. Fluid Mech.*, 178:459–475, 1987.

[24] P. van Beek, R.R.P. van Nooyen, and P. Wesseling. Accurate discretization on non-uniform curvilinear staggered grids. *J. Comp. Phys.*, 117:364–367, 1995.

[25] J.J.I.M. Van Kan. A second-order accurate pressure correction method for viscous incompressible flow. *SIAM J. Sci. Stat. Comp.*, 7:870–891, 1986.

[26] C. Vuik. Solution of the discretized incompressible Navier-Stokes equations with the GMRES method. *Int. J. for Num. Meth. Fluids*, 16:507–523, 1993.

[27] C. Vuik. Fast iterative solvers for the discretized incompressible Navier-Stokes equations. *Int. J. for Num. Meth. Fluids*, 22:195–210, 1996.

[28] P. Wesseling, C.G.M. Kassels, C.W. Oosterlee, A. Segal, C. Vuik, S. Zeng, and M. Zijlema. Computing incompressible flows in general domains. In F.-K. Hebeker, R. Rannacher, and G. Wittum, editors, *Numerical methods for the Navier-Stokes equations*, pages 298–314, Braunschweig, 1994. Vieweg.

[29] P. Wesseling, A. Segal, J.J.I.M. van Kan, C.W. Oosterlee, and C.G.M. Kassels. Finite volume discretization of the incompressible Navier-Stokes equations in general coordinates on staggered grids. *Comp. Fluid Dynamics Journal*, 1:27–33, 1992.

[30] P. Wesseling, M. Zijlema, A. Segal, and C.G.M. Kassels. Computation of turbulent flow in general domains. Report 95-85, Delft University of Technology, Faculty of Technical Mathematics and Informatics, Delft, The Netherlands, 1995.

[31] D.C. Wilcox. Reassessment of the scale determining equation for advanced turbulence models. *AIAA J.*, 26:1299–1310, 1988.

[32] V. Yakhot, S.A. Orszag, S. Thangam, T.B. Gatski, and C.G. Speziale. Development of turbulence models for shear flows by a double expansion technique. *Phys. Fluids A*, 4:1510–1520, 1992.

[33] S. Zeng and P. Wesseling. Multigrid solution of the incompressible Navier-Stokes equations in general coordinates. *SIAM J. Num. Anal.*, 31:1764–1784, 1994.

[34] M. Zijlema. *Computational modeling of turbulent flow in general domains*. PhD thesis, Delft University of Technology, Delft, 1996.

[35] M. Zijlema, A. Segal, and P. Wesseling. Finite volume computation of incompressible turbulent flows in general coordinates on staggered grids. *Int. J. Numer. Meth. Fluids*, 20:621–640, 1995.

[36] M. Zijlema, A. Segal, and P. Wesseling. Invariant discretization of the k-ε model in general co-ordinates for prediction of turbulent flow in complicated geometries. *Comput. Fluids*, 24:209–225, 1995.

[37] M. Zijlema and P. Wesseling. Higher order flux-limiting methods for steady-state, multidimensional, convection-dominated flow. Report 95-131, Delft University of Technology, Faculty of Technical Mathematics and Informatics, Delft, The Netherlands, 1995.